ORIGINAL ARTICLE

In situ Fabrication and Photocatalytic Performance of CeO_2/Fe_2O_3 Core-Shell Decorated rGO Nanocomposites

K. Satyam Naidu[1], Nowduri Annapurna[2], R. S. K. Sharma[1], G. V. SivaPrasad[1], M. RaviKumar[1]

[1]Department of Chemistry, Raghu Engineering College, Visakhapatnam, Andhra Pradesh, India, [2]Department of Engineering Chemistry, Andhra University, AU College of Engineering, Visakhapatnam, Andhra Pradesh, India

Abstract

Introduction: This study investigates the *in situ* fabrication, characterization, and photocatalytic efficiency of CeO_2/Fe_2O_3 core-shell decorated reduced graphene oxide (rGO) nanocomposites for degrading organic pollutants. **Materials and Methods:** All chemicals were of analytical grade and used without further purification. CeCl3.7H2O and FeSO4.7H2O were dissolved in a 1:1 ratio in 50 mL of double-distilled water, followed by the addition of 0.1 M urea and 0.1 g of as-prepared GO. The solution was ultra-sonicated for 30 min, stirred for 1 h, and then heated at 180°C for 18 h in an autoclave. The precipitate was washed, dried, and calcined at 400°C for 2 h to obtain the CeO_2/Fe_2O_3/r-GO nanocomposite. Photocatalytic activity was tested using 100 mg of the catalyst in 100 mL dye solutions of Indigo Carmine and Eosin Blue (1×10^{-5} M), with pH adjustments. The mixture was stirred for 3 h under visible light from a 200 W tungsten lamp. Dye degradation was monitored by measuring absorbance at 557 nm with a Ultraviolet–visible (UV–Vis) spectrophotometer, and degradation efficiency was calculated. **Results and Discussion:** The successful synthesis of CeO_2/Fe_2O_3/rGO nanocomposites has shown notable improvements in photocatalytic performance, primarily due to enhanced electron-hole separation and adsorption properties from rGO. Characterizations confirmed efficient charge transfer and reduced recombination rates. UV-Vis spectroscopy and X-ray diffraction validated the nanocomposites' structural integrity. Photocatalytic tests demonstrated high degradation efficiencies of 86% for Indigo Carmine and 92% for Eosin Blue under sunlight, highlighting their potential for environmental remediation. These results underscore the promise of CeO_2/Fe_2O_3/rGO nanocomposites in sustainable technologies for environmental cleanup and industrial applications. **Conclusion:** CeO_2/Fe_2O_3/rGO offering an effective and sustainable solution for organic dye degradation in water under visible light irradiation.

Key words: Graphene-based nanocomposites, CeO_2/Fe_2O_3/r-GO, co-precipitation method, photocatalytic degradation, indigo carmine, eosin blue, nanocomposite materials

INTRODUCTION

This study investigates the *in situ* fabrication and photocatalytic performance of CeO_2/Fe_2O_3 core-shell decorated reduced graphene oxide (rGO) nanocomposites. The research focuses on synthesizing these nanocomposites using a specific method and comprehensively characterizing their structural and optical properties. Photocatalytic experiments will evaluate their efficiency in degrading organic pollutants under simulated environmental conditions. CeO_2/Fe_2O_3/rGO nanocomposites leverage CeO_2 and Fe_2O_3's photocatalytic properties, enhanced by rGO's electron transfer and surface area capabilities. *In situ* fabrication methods optimize material integration for synergistic effects, enhancing efficacy in environmental remediation and industrial processes. Understanding their structural design and photocatalytic mechanisms is crucial for advancing sustainable technologies. Water pollution and the energy crisis are significant challenges today, impacting human well-being. Industrial discharge of organic dyes poses severe environmental and health risks, including

Address for correspondence:
K. Satyam Naidu, Department of Chemistry, Raghu Engineering College, Visakhapatnam, Andhra Pradesh, India. Phone: 9100696914.
E-mail: ksatyam58@gmail.com

Received: 14-08-2024
Revised: 29-10-2024
Accepted: 15-11-2024

carcinogenicity.[1,2] Effective photocatalytic catalysts are developed to purify contaminated water under sunlight. CeO_2 stands out for its wide bandgap (2.5 – 3.1 eV), strong photo-response, and oxygen vacancies that enhance visible light photo catalysis.[3-7] Composite materials, such as Fe_2O_3/CeO_2 and BiVO4/CeO_2 improve photocatalytic performance by mitigating electron-hole recombination.[8-12] Doping or combining CeO_2 with other elements optimizes its efficacy in environmental clean-up and sustainable technology applications.[13]

CeO_2/Fe_2O_3/r-GO nanocomposites were synthesized through co-precipitation and annealing to enhance photocatalytic performance. Previous research highlights the effectiveness of coupling CeO_2 with iron oxide to improve charge separation efficiency, crucial for photocatalytic activity.[14,15] Graphene oxide (GO) was incorporated to enhance visible light photo catalysis through its structural features and conductivity, facilitating efficient electron transport and minimizing charge carrier recombination.[16-22] The synthesized CeO_2/Fe_2O_3/r-GO nanocomposites, characterized by X-ray diffraction (XRD), Energy dispersive X-ray spectroscopy (EDX), HR-transmission electron microscopy (TEM), Ultraviolet–visible (UV-Vis) DRS and X-ray photoelectron spectroscopy (XPS), showed significant degradation of Indigo carmine and Eosin blue under UV light. Stability tests confirmed their robustness over five cycles, highlighting their potential in water treatment. The fabrication involved synthesizing CeO_2 nanoparticles, creating a Fe_2O_3 core-shell structure, and integrating rGO. The photocatalytic performance, evaluated under simulated sunlight or UV light, and the stability and recyclability were assessed through multiple cycles. These methods aim to optimize fabrication and understand photocatalytic mechanisms for environmental applications.[23-26]

MATERIALS AND METHODS

Materials

All chemicals used were of analytical grade and employed without further purification for dye degradation experiments. Graphite flakes, ferrous sulphate FeSO4.7H2O cerium chloride CeCl3.7H2O and urea were purchased from Sigma-Aldrich.

Nanofabrication techniques

Preparation of The CeO_2/Fe_2O_3/R-GO nanocomposite $CeCl_3.7H_2O$ and $FeSO_4.7H_2O$ were dissolved in a 1:1 stoichiometric ratio in 50 mL of double-distilled water. A 0.1 M urea (CH_4N_2O) solution was then added to the mixture, followed by the addition of 0.1 g of as-prepared GO. The solution was ultra-sonicated for 30 min and stirred continuously for 1 h. The mixture was transferred to a 100 mL autoclave and heated at 180°C for 18 h. The resulting precipitate was collected, washed with DI water and ethanol, dried in an oven, and finally calcined at 400°C for 2 h to yield the CeO_2/Fe_2O_3/r-GO hybrid nanocomposite.

Photo-catalytic activity measurements

The photodegradation performance of the CFG hybrid Nano catalyst was assessed using Indigo carmine and Eosin blue as model pollutants. In each experiment, 100 mg of the catalyst was mixed with 100 mL of a dye solution (1×10^{-5} M) in a 250 mL beaker. The pH of the dye solutions was adjusted with dilute HCl and NaOH. The dye-catalyst mixture was stirred for 3 h to reach adsorption-desorption equilibrium. Visible light irradiation was provided by a 200 W tungsten lamp positioned 20 cm above the reaction vessel. Aliquots (3 mL) were taken at regular intervals, centrifuged at 4700 rpm for 10 min, and the absorbance of the supernatant was measured at 557 nm using a UV–Vis spectrophotometer to monitor dye concentration changes. The degradation efficiency (η) was calculated using $\eta = (C_0 - C)/C_0 \times 100$, where C_0 is the initial dye concentration and C is the concentration after photo degradation. CFG catalyst Represents Cerium (Ce), Iron (Fe), and Oxides (Ox). rGO: Reduced Graphene Oxide composite catalyst

These above equations effectively summarize the key steps involved in the photocatalytic processes of CeO_2, Fe_2O_3, and rGO under light irradiation. They illustrate the generation of electron-hole pairs, subsequent charge transfer processes between the materials, and the formation of reactive oxygen species (ROS), such as superoxide radicals. These ROS play a significant role in degrading organic dye pollutants, making this photocatalytic system highly effective for environmental remediation applications. The table highlights the intricate interactions and reactions that drive the degradation process, emphasizing the efficiency and potential of this photocatalytic approach.

The photocatalytic processes involving CeO_2, Fe_2O_3, and rGO under light irradiation have been effectively elucidated through a series of chemical equations. These processes highlight the generation of electron-hole pairs, efficient charge transfer between materials, and the formation of reactive oxygen species (ROS) such as superoxide radicals. The synergy between CeO_2, Fe_2O_3, and rGO enhances the overall photocatalytic activity, leading to significant degradation of organic dye pollutants. This study demonstrates the potential of this photocatalytic system for environmental remediation, offering a sustainable and efficient method for pollutant degradation. The detailed mechanistic insights provided by the equations emphasize the critical roles of electron-Hole dynamics and ROS formation in achieving effective photocatalytic performance.

Characterization

PXRD of GO, CeO_2, Fe_2O_3, CeO_2/Fe_2O_3/r-GO hybrid nanocomposite

To determine the crystallite sizes and identify the phases of the CeO_2/Fe_2O_3/r-GO nanocomposite, XRD analysis was performed at room temperature using an X-ray diffractometer

with Cu Kα radiation (λ = 1.54 Å). The average crystallite sizes were calculated using Scherer's formula.

$$D = \frac{0.94\ \lambda}{\beta Cos\theta}$$

Here, D represents the crystalline size, λ is the wavelength of incident X-rays (1.54 Å), θ is the diffraction angle, and β is the FWHM. The average crystalline size of CeO_2/Fe_2O_3/r-GO nanocomposite has a size of 29.2 nm, likely due to the integration of r-GO during composite formation. The XRD diffraction patterns of CeO_2, Fe_2O_3, and CeO_2/Fe_2O_3/r-GO nanocomposites are shown in Figure 1. The CeO_2 peaks at 29.3, 33.02, 44.36, 56.10, 59.12, 68.38, 76.40, and 78.19 correspond to the (111), (200), (220), (311), (222), (400), (331), and (420) planes of fluorite CeO_2 (JCPDS card no. 34-0394). The Fe_2O_3 peaks at 24.24, 24.6, 33.07, 35.59, 40.75, 49.47, 54.15, 57.47, 62.32, 63.88, 72.24, and 75.27 correspond to the (012), (120), (104), (110), (113), (024), (116), (214), (300), (119), and (220) planes of rhombohedral Fe_2O_3 (JCPDS card no. 89-0599). In addition, the r-GO broad peak at 2θ = 26.2 corresponds to the (002) plane of r-GO (JCPDS card no. 75-1621) Figure 1.

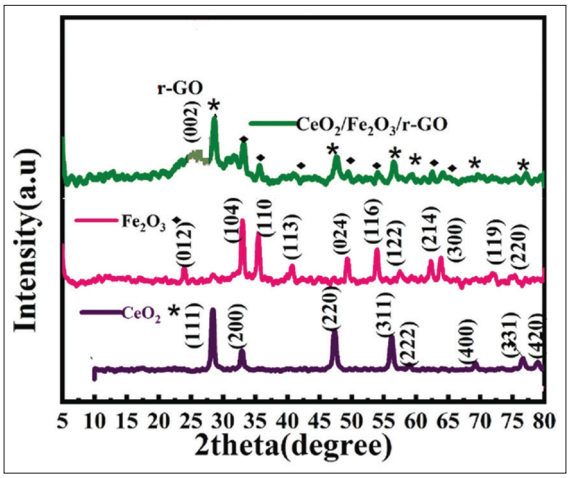

Figure 1: X-ray diffraction spectra of GO, CeO_2, Fe_2O_3, CeO_2/Fe_2O_3/r-GO hybrid nanocomposite

EDX analysis

EDX analysis confirmed the presence of C, O, Fe, and Ce on the CeO_2/Fe_2O_3/r-GO nanocomposite surface. The elemental ratio was found to be C: O: Fe= 66.29: 11.80: 13.28: 8.63. Further calculations revealed a CeO_2 to Fe_2O_3 ratio of 1.53, indicating the formation of both binary oxides on the graphene sheets. XPS analysis indicated average mole fractions of 41.1% Ce, 25.2% Fe, 27.1% carbon, and 6.43% oxygen in the analysed area. These findings were supported by HR-TEM and EDX studies, which confirmed the purity and elemental composition observed in XRD results Figure 2.

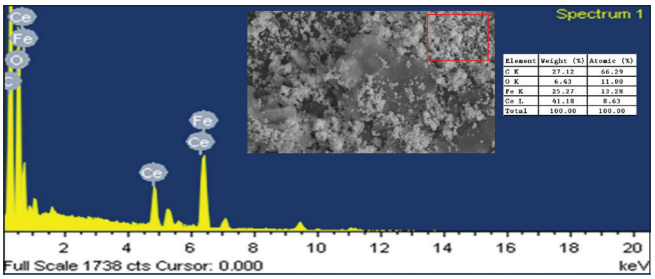

Figure 2: The Energy dispersive X-ray spectroscopy image of CeO_2/Fe_2O_3/r-GO nanocomposite

TEM examination

TEM images shown in figure 3a-3c illustrate the morphology of pure CeO_2, pure Fe_2O_3, and CeO_2/Fe2 O3 /r-GO, respectively. Figure 3a shows non-uniformly agglomerated CeO_2 nanocrystals, while Figure 3b reveals homogeneously dispersed hexagonal Fe_2O_3 nanocrystals. No secondary phase peaks were observed. TEM images of the CeO_2/Fe_2O_3/r-GO composite [Figure 3c] indicate the average particle size 30 nm for the composite. These observations are consistent with crystallite sizes calculated by Scherer's formula from XRD data Figure 3.

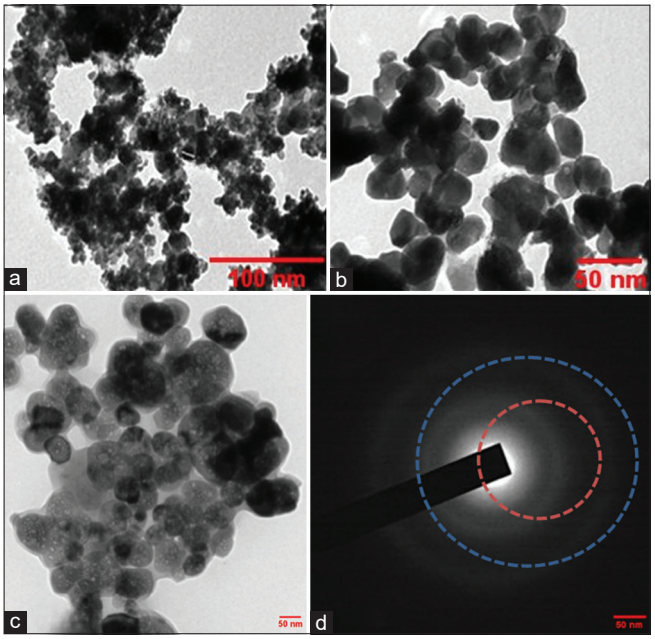

Figure 3: Transmission electron microscopy examination of (a) pure CeO_2 nanoparticles, (b) pure FeO_2 and (c) CeO_2/Fe_2O_3/r-GO Composite (d) SAED of CeO_2/Fe_2O_3/r-GO

UV–DRS spectra

The UV–DRS spectra of CeO_2, Fe_2O_3, and CeO_2/Fe_2O_3/r-GO nanocomposites exhibited enhanced absorption in visible light, notably stronger than other composite materials. CeO_2/Fe_2O_3/r-GO showed increased absorbance around 600–610 nm, correlating with observed color changes. Bandgap analysis revealed values of 2.5 eV for CeO_2, 1.91 eV for Fe_2O_3, and 1.87 eV for CeO_2/Fe_2O_3/r-GO, indicating a decreased bandgap in the nanocomposite, likely due to r-GO incorporation. This reduction enhances photocatalytic

activity by facilitating charge transfer, thereby promoting efficient visible light utilization. Figure 4.

XPS analysis

The chemical components of as-synthesized CeO_2/Fe_2O_3/r-GO nanocomposite were explored through XPS. Figure 5a demonstrates the survey spectrum of CeO_2/Fe_2O_3/r-GO nanocomposite which clearly confirms the presence of Ce, Fe, O, and C elements. Figure 5b displays the DE convoluted spectra of Ce and it is well matched with the corresponding binding energies are Ce 3d3/2 (904 eV) and Ce 3d5/2 (891 eV), respectively. Figure 5(c-e) are DE convoluted spectra of C, Fe & O.

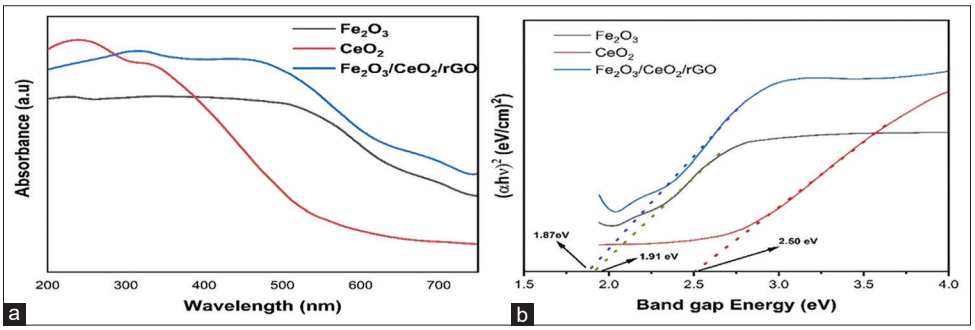

Figure 4: (a) Ultraviolet–visible diffuse reflectance spectroscopy spectra, (b) Tauc plot of Band gaps of CeO_2, Fe_2O_3, CeO_2/Fe_2O_3 and CeO_2/Fe_2O_3/r-GO hybrid nanocomposite

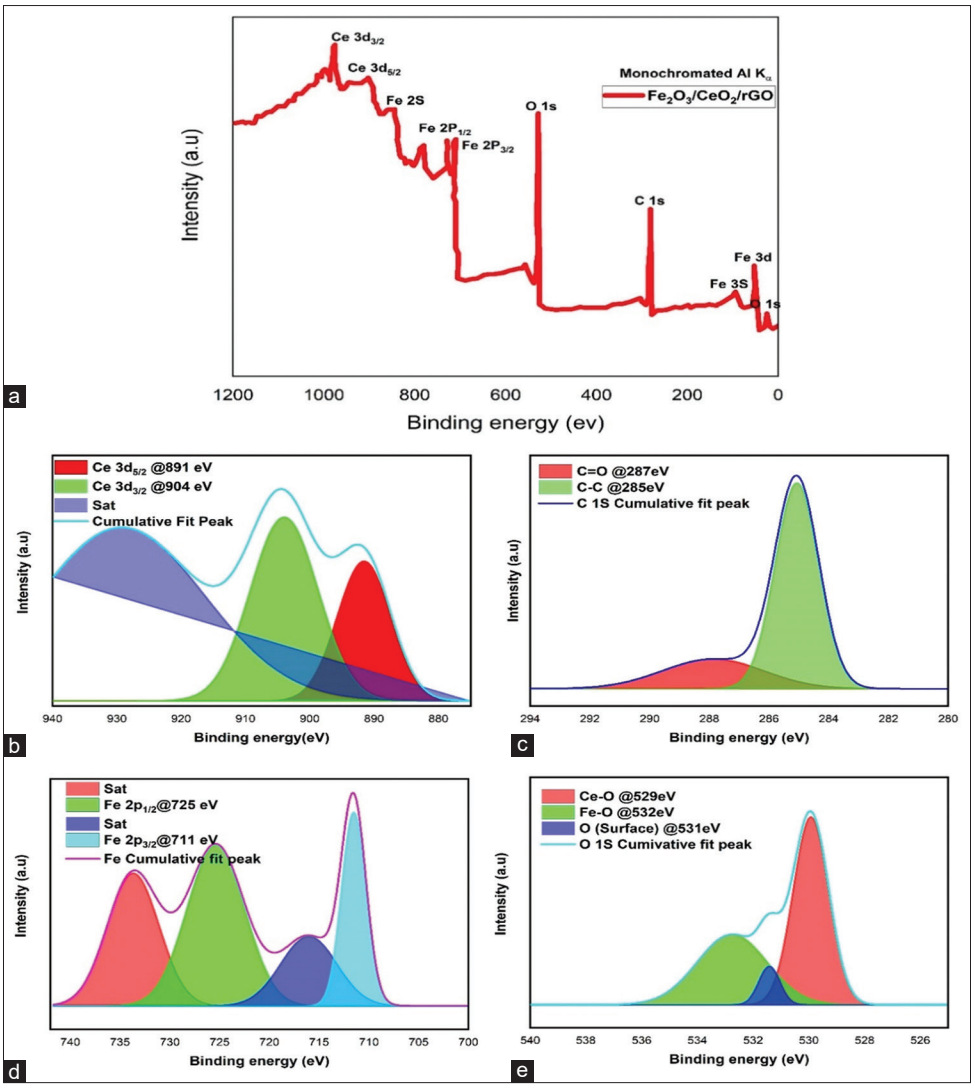

Figure 5: XPS spectrum (a) XPS of CeO_2/Fe_2O_3/r-GO hybrid nanocomposite (b) DE convoluted spectra of Ce, (c) DE convoluted spectra of C, (d) DE convoluted spectra of Fe and (e) DE convoluted spectra of O. XPS: X-ray photoelectron spectroscopy

Figure 6 photocatalytic degradation of indigo carmine dye. The study investigated the photocatalytic performance of CeO_2/Fe_2O_3/r-GO hybrid nanocomposites using Indigo Carmine dye. (a) UV-vis absorption spectra recorded the evolution of absorption characteristics over time under irradiation. (b) Changes in the relative concentration of Indigo Carmine were analyzed as a function of irradiation duration. (c) The relationship between irradiation time and $\ln(C/C_0)$ provided insights into the degradation kinetics, showcasing the catalyst's efficiency. (d) Photocatalytic efficiency assessments demonstrated the effectiveness of CeO_2/Fe_2O_3/r-GO in degrading Indigo Carmine, highlighting its potential for environmental remediation applications.

Figure 7 photocatalytic degradation of eosin blue dye. The study investigated the photocatalytic performance of CeO_2/Fe_2O_3/r-GO hybrid nanocomposites using Eosin blue.

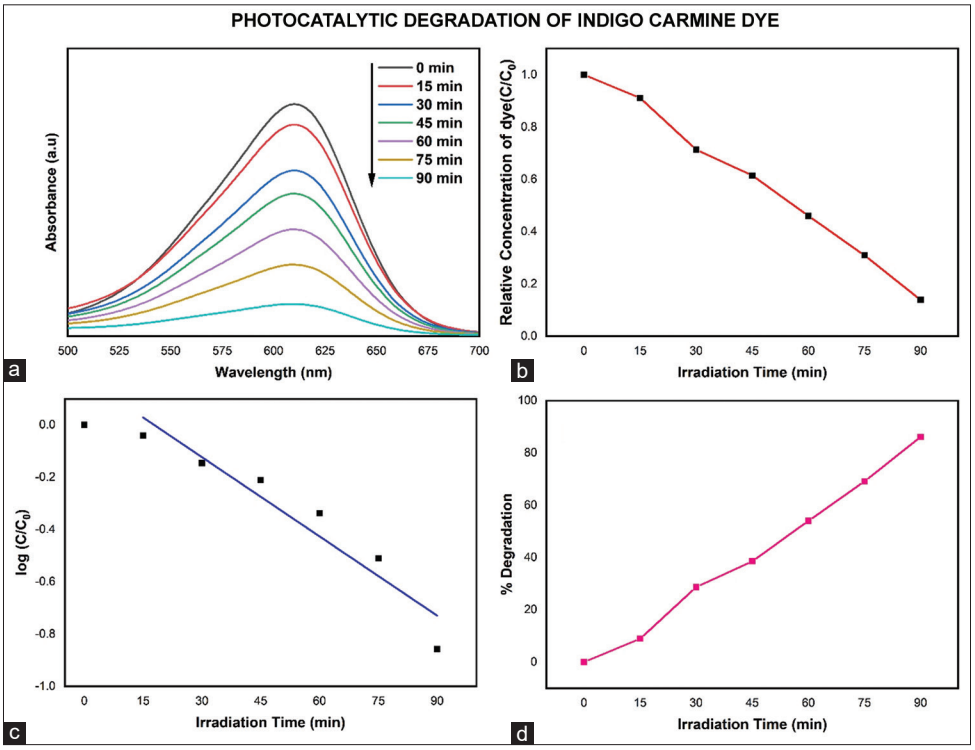

Figure 6: The study investigated the photocatalytic performance of CeO_2/Fe_2O_3/r-GO hybrid nanocomposites using indigo carmine dye

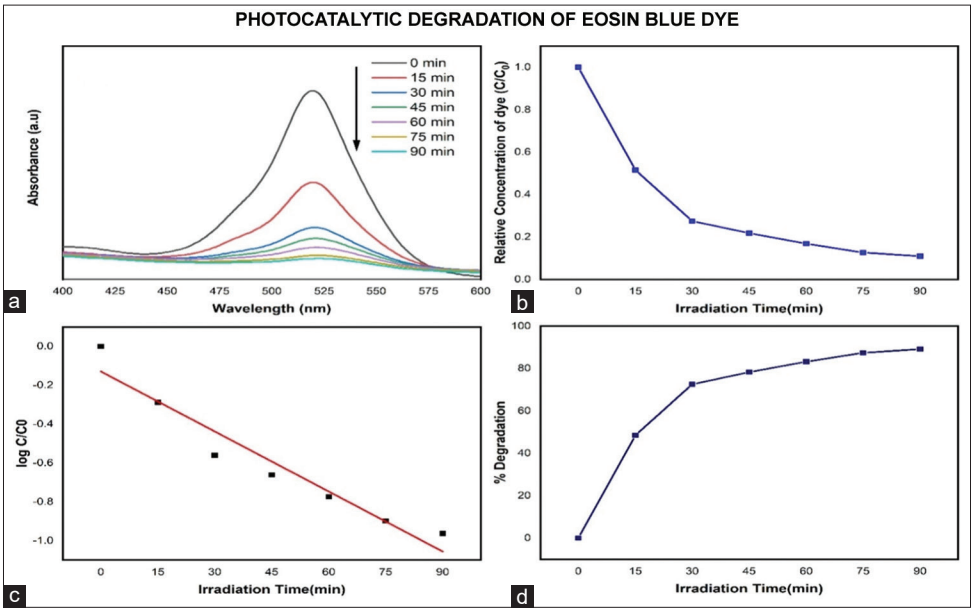

Figure 7: The study investigated the photocatalytic performance of CeO_2/Fe_2O_3/r-GO hybrid nanocomposites using eosin blue

(a) UV-vis absorption spectra of Eosin Blue for the CeO_2/Fe_2O_3/r-GO hybrid nanocomposite were recorded over irradiation time, (b) The relationship between relative concentration of Eosin Blue and irradiation time was analyzed.

(c) Irradiation time versus $\ln(C/C_0)$ provided insights into the degradation kinetics, (d) the photocatalytic efficiency of CeO_2/Fe_2O_3/r-GO for Eosin Blue demonstrated effective degradation, highlighting its potential for practical applications in environmental remediation.

Animals

Not applicable.

Recovery study

Recyclability and stability are critical factors for the practical application of CeO_2/Fe_2O_3/r-GO hybrid nanocomposites in photocatalysis, especially in environmental remediation. This study systematically evaluated the photocatalytic activity of the nanocomposite by conducting five successive cycles of degrading two commonly used dyes: Indigo Carmine and Eosin Blue. Each cycle involved exposing the dyes to the photo catalyst for 90 min, after which the nanocomposite was thoroughly washed to remove any residual dye and other by-products. The washed catalyst was then reused in the next cycle. This rigorous testing method aimed to simulate real-world conditions where catalysts are repeatedly used over time.

The results demonstrated that the CeO_2/Fe_2O_3/r-GO nanocomposite maintained a high level of photocatalytic efficiency throughout the cycles. There was only a minor decrease in activity, which was attributed primarily to the physical washing process and the adhesion of dye molecules on the catalyst's surface. Despite these minor losses, the overall performance remained robust, underscoring the nanocomposite's durability and efficiency. The stability of the photocatalytic activity over multiple cycles indicates that the CeO_2/Fe_2O_3/r-GO hybrid nanocomposite is not only effective in degrading harmful dyes but also possesses the resilience necessary for long-term use. This characteristic is vital for practical applications, as it reduces the need for frequent replacement or regeneration of the catalyst, thereby lowering operational costs and enhancing sustainability.

Furthermore, the study's findings suggest that this nanocomposite could be a viable candidate for large-scale environmental clean-up efforts. Its ability to consistently perform over multiple cycles without significant loss of activity highlights its potential for practical, real-world applications where stable and recyclable photo catalysts are essential for efficient and cost-effective pollutant degradation.

Figure 8 recyclability of catalyst for (a) indigo carmine and (b) eosin blue dye.

RESULTS AND DISCUSSION

The successful synthesis of the CeO_2/Fe_2O_3/rGO nanocomposite has been achieved, showcasing significant advancements in photocatalytic performance. The observed enhancement in activity can be attributed primarily to the improved separation of electron-hole pairs and the enhanced adsorption properties introduced by the presence of rGO.

Structural and functional characterization

The comprehensive characterization of the CeO_2/Fe_2O_3/rGO nanocomposite through XRD, EDX, TEM, UV-Vis DRS, and XPS analyses provides a detailed understanding of its structural, compositional, and optical properties. The XRD and EDX analyses confirmed the successful synthesis and elemental composition, while TEM images revealed the well-dispersed nanoparticles. UV-Vis DRS demonstrated enhanced light absorption capabilities, and XPS provided insights into the strong interactions within the composite. These combined characterizations underscore the potential of the CeO_2/Fe_2O_3/rGO nanocomposite for efficient and sustainable photocatalytic applications.

XRD analysis

XRD analysis was employed to determine the crystalline structure of the CeO_2/Fe_2O_3/rGO nanocomposite. The XRD patterns confirmed the successful incorporation of CeO_2 and Fe_2O_3 into the rGO matrix, revealing distinct diffraction peaks corresponding to the crystallographic planes of CeO_2 and Fe_2O_3. The sharp and well-defined peaks indicate a high degree of crystallinity, which is essential for efficient photocatalytic activity. The Absence of any impurity peaks further corroborates the purity and successful synthesis of the composite material.

EDX analysis

EDX was utilized to analyze the elemental composition of the nanocomposite. EDX mapping showed a uniform distribution of Ce, Fe, O, and C elements, confirming the homogeneous dispersion of CeO_2 and Fe_2O_3 nanoparticles on the rGO sheets. This uniform distribution is crucial for ensuring consistent photocatalytic performance across the material. The quantitative EDX analysis provided precise elemental ratios, further verifying the stoichiometry of the synthesized nanocomposite.

TEM analysis

TEM provided high-resolution images of the nanocomposite, revealing the detailed morphology and structural arrangement. TEM images showed well-dispersed CeO_2 and Fe_2O_3 nanoparticles uniformly anchored onto the rGO

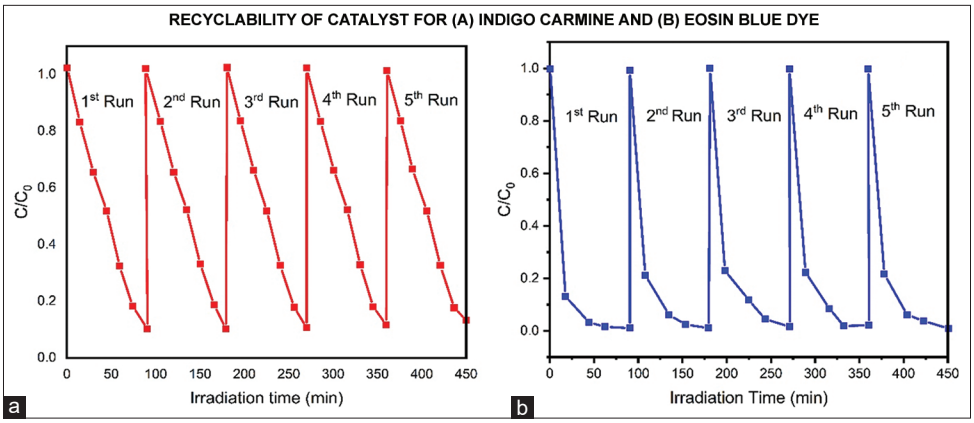

Figure 8: The cyclic testprofiles of catalyst in reaction for recyclability of (a) indigo carmine (b) eosin blue

sheets. The nanoparticles exhibited sizes in the nanometer range, which is beneficial for maximizing the surface area available for photocatalytic reactions. The intimate contact between the nanoparticles and rGO sheets observed in TEM images indicates efficient charge transfer pathways, crucial for reducing electron-hole recombination rates.

UV-Vis diffuse reflectance spectroscopy (UV-Vis DRS) analysis

UV-Vis DRS was used to investigate the optical properties of the nanocomposite. The UV-Vis DRS spectrum showed a broadened absorption band extending into the visible light region, indicating enhanced light-harvesting capabilities. This broad absorption is attributed to the presence of rGO, which enhances the absorption of light across a wider range of wavelengths. The improved light absorption is expected to enhance the photocatalytic activity of the nanocomposite by generating more electron-hole pairs under solar irradiation.

XPS analysis

XPS was conducted to investigate the surface chemical states and interactions within the nanocomposite. XPS spectra revealed the presence of Ce 3d, Fe 2p, O 1s, and C 1s peaks, confirming the presence of CeO_2, Fe_2O_3, and rGO. The binding energy shifts observed in the XPS spectra indicated strong interactions between rGO and the metal oxides, which are crucial for efficient charge separation and transfer. The reduced recombination rates of photogenerated charge carriers are attributed to these strong interactions, as evidenced by the XPS analysis.

Degradation efficiency

Photocatalytic tests conducted under sunlight irradiation reveal that the CeO_2/Fe_2O_3/rGO nanocomposite achieves significantly higher degradation efficiencies for organic dyes. Specifically, the nanocomposite demonstrated a degradation efficiency of 86% for indigo carmine dye and 92% for eosin blue dye within a 90-min exposure period [Table 2].

Photocatalytic degradation

The comprehensive analysis of the photocatalytic degradation of both Indigo Carmine and Eosin Blue dyes using CeO_2/Fe_2O_3/r-GO hybrid nanocomposites underscores their potential for environmental cleanup applications. The studies demonstrated that these nanocomposites exhibit high degradation efficiencies, effective degradation kinetics, and strong photocatalytic performance under irradiation. These results advocate for the broader application of CeO_2/Fe_2O_3/r-GO nanocomposites in environmental remediation technologies, leveraging their unique properties to achieve sustainable and efficient pollutant degradation.

The study demonstrated the photocatalytic performance of CeO_2/Fe_2O_3/r-GO nanocomposites in degrading indigo carmine and eosin dye. UV-Vis spectroscopy revealed a gradual decrease in absorption peak intensity over time, indicating effective dye breakdown. Relative concentration analysis showed a significant reduction in dye concentration, highlighting the composite's photocatalytic activity. Degradation kinetics, plotted as $\ln(C/C_0)$ versus irradiation time, confirmed pseudo-first-order kinetics and high catalyst efficiency. Overall, the assessments underscored the remarkable effectiveness of CeO_2/Fe_2O_3/r-GO in environmental remediation, offering a sustainable solution for dye pollutant removal.

Photocatalytic degradation of eosin blue dye

The photocatalytic performance of CeO_2/Fe_2O_3/r-GO nanocomposites for degrading Eosin Blue dye was evaluated using UV-Vis spectroscopy, which showed a significant reduction in absorption peak intensity, indicating efficient dye degradation. Relative concentration analysis confirmed a notable decline in dye concentration over time, while degradation kinetics supported pseudo-first-order behavior, highlighting the catalyst's effectiveness. Overall, the high

Table 1: Photocatalytic processes of CeO_2, Fe_2O_3, and rGO under visible light irradiation

Step	Process description	Chemical equation
1	Photoexcitation of CeO_2	$CeO_2+h\nu \rightarrow CeO_2 (e^- + h^+)$
2	Photoexcitation of Fe_2O_3	$Fe_2O_3+h\nu \rightarrow Fe_2O_3 (e^- + h^+)$
3	Electron-Hole Recombination	$e^- + h^+ \rightarrow$ Heat
4	Photoexcitation of rGO	$rGO+h\nu \rightarrow rGO^*$
5	Electron Transfer from rGO to Fe_2O_3	$rGO^* + Fe_2O_3 \rightarrow Fe_2O_3 (e^-) + rGO^*)$
6	Electron Transfer from Fe_2O_3 to CeO_2	$Fe_2O_3 (e^-) + CeO_2 \rightarrow CeO_2 (e^-) + Fe_2O_3$
7	Hole Transfer from CeO_2 to Fe_2O_3	$CeO_2 (h^+) + Fe_2O_3 \rightarrow Fe_2O_3 (h^+) + CeO_2$
8	Reduction of Oxygen	$O_2+e- \rightarrow O_2\bullet-$
9	Degradation of Dye by Holes and Superoxide Radicals	h+, $O_2\bullet-$+ dye→Degraded products

The table 1 outlines the photocatalytic processes of CeO_2, $Fe2O_3$, and rGO under light irradiation, illustrating electron-hole dynamics and dye degradation mechanisms

Table 2: Photocatalytic degradation efficiency of $CeO_2/Fe2O_3$/rGO nanocomposite

Dye	Initial concentration (mg/L)	Degradation efficiency (%)
Indigo carmine	10	86
Eosin blue	10	92

degradation efficiency underscores the nanocomposites' potential for practical environmental remediation applications.

Synergistic effects and environmental implications

The synergistic effects of rGO, CeO_2, and Fe_2O_3 not only enhance photocatalytic performance but also promote the sustainability of remediation technologies. The rGO component provides a large surface area for adsorption, enhances light absorption, and facilitates electron transport, thereby optimizing the separation and transfer of photo generated charge carriers. The combination of CeO_2 and Fe_2O_3 results in superior photocatalytic activity due to improved charge separation and minimized recombination rates.

Future directions and recommendations

Optimization of synthesis process

Future research should focus on optimizing the synthesis process to further enhance the photocatalytic performance and scalability of CeO_2/Fe_2O_3/rGO nanocomposites. Investigations into different rGO loadings and exploring other metal oxide combinations could yield even more efficient photo catalysts.

Long-term stability and real-world applications

Conducting long-term stability tests and real-world application trials will be essential to fully establish the practical viability of these nanocomposites in environmental cleanup efforts. Assessing the performance of the nanocomposite in degrading other types of pollutants, including heavy metals and pharmaceuticals, can broaden its application scope.

Environmental and economic impact

Analyzing the environmental and economic impact of large-scale deployment of CeO_2/Fe_2O_3/rGO nanocomposites can provide valuable insights into their sustainability and cost-effectiveness. Exploring methods for the regeneration and recycling of the nanocomposite to maintain its long-term activity and reduce waste generation.

The photocatalytic efficiency of the CeO_2/Fe_2O_3/rGO nanocomposite under visible light is significantly improved due to the effective band alignment between its components. The absolute electronegativities of CeO_2 and Fe_2O_3 are 5.56 eV and 5.87 eV, respectively, which directly influence their band structure and interaction within the hybrid system. For CeO_2, the conduction band (CB) and valence band (VB) energies are calculated to be −0.24 eV and 2.26 eV, respectively. In contrast, Fe_2O_3 has CB and VB energies of 0.24 eV and 2.15 eV. In this hybrid system, photo-induced electrons excited to the CB of CeO_2 migrate to the lowest unoccupied molecular orbital of rGO. rGO acts as an effective electron conduit, facilitating the transfer of these electrons to the CB of Fe_2O_3. This electron transfer mechanism is crucial as it minimizes charge carrier recombination by effectively separating the photo generated electron-hole pairs.

The role of rGO in this system is pivotal; it not only bridges the electron transfer between CeO_2 and Fe_2O_3 but also helps in forming reactive radicals that are essential for the photocatalytic degradation process. The reduced recombination rates of charge carriers lead to enhanced photocatalytic activity by ensuring that more electrons and holes are available for reaction, thus increasing the formation of potential radicals that drive the degradation of contaminants. This efficient charge transfer and radical generation are illustrated in the bandgap alignment shown in Figure 9, which visually represents how the band energies and the presence of rGO contribute to the improved photocatalytic

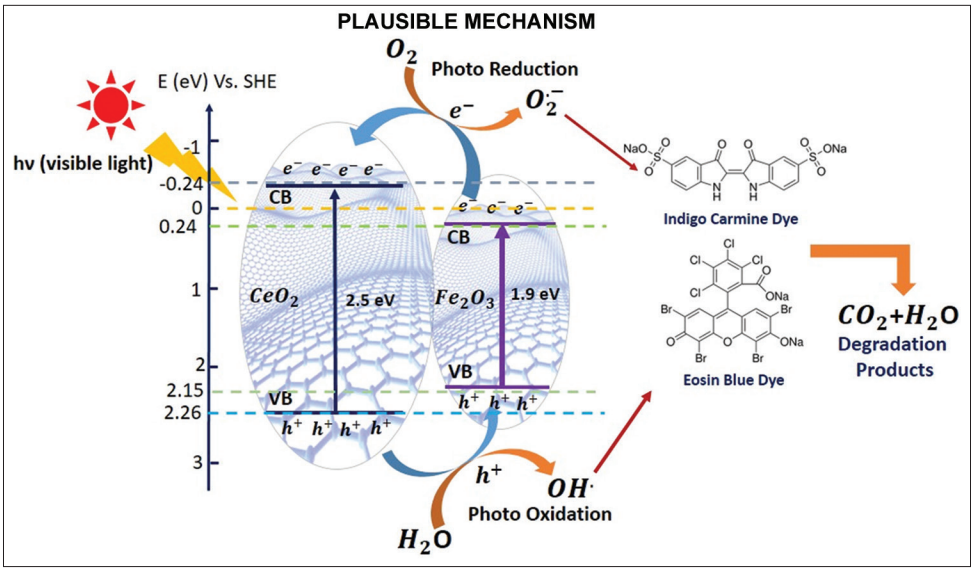

Figure 9: The band edge positions of the conduction band (CB) and valence band (VB) of the CeO_2/Fe_2O_3/rGO nanocomposite can be determined using the following equations

$E_{CB} = \chi - E_{ef} - 0.5\ E_g$

$E_{VB} = ECB + E_g$

performance of the CeO_2/Fe_2O_3/rGO nanocomposite. The effective band alignment and charge separation enabled by this hybrid system are key factors driving its superior photocatalytic efficiency under visible light.

CONCLUSION

The graphene-based CFG nanocomposite, synthesized through co-precipitation, exhibits significantly enhanced photocatalytic performance. This enhancement is attributed to improved electron-hole pair separation and increased adsorption capabilities due to the presence of rGO. Structural characterization confirmed the integrity and stability of the nanocomposite. The composite demonstrated high photocatalytic efficiency, achieving 86% degradation of Indigo Carmine and 92% degradation of Eosin Blue under UV light, along with excellent recyclability over five cycles. These findings indicate that the CeO_2/Fe_2O_3/rGO nanocomposite holds great promise for both environmental and industrial applications, offering an effective and sustainable solution for organic dye degradation in water under sunlight irradiation.

ACKNOWLEDGMENT

The authors extend sincere gratitude to Department of Engineering Chemistry at Andhra University and the Department of Chemistry at Raghu Engineering College, Visakhapatnam, for their invaluable contributions and insightful scientific discussions. In addition, we acknowledge the steadfast support from the authorities of Raghu Engineering College, which has been integral to the successful completion of this work.

FUNDING

Nil.

CONFLICTS OF INTEREST

All authors confirm that there are no conflicts of interest and financial interests relevant to this research work.

REFERENCES

1. Corredor J, Rivero MJ, Rangel CM, Gloaguen F, Ortiz I. Comprehensive review and future perspectives on the photocatalytic hydrogen production. J Chem Technol Biotechnol 2019;94:3049-63.
2. Zhang W, Li G, Liu H, Chen J, Maa S, An T. Micro/nano-bubble assisted synthesis of Au/TiO_2@CNTs composite photocatalyst for photocatalytic degradation of gaseous styrene and its enhanced catalytic mechanism. Environ Sci Nano 2019;6:948-58.
3. Gómez V, Larrechi MS, Callao MP. Kinetic and adsorption study of acid dye removal using activated carbon. Chemosphere 2007;69:1151-8.
4. Khataee AR, Kasiri MB. Photocatalytic degradation of organic dyes in the presence of nanostructured titanium dioxide: Influence of the chemical structure of dyes. J Mol Catal A Chem 2010;328:8-26.
5. Poulios I, Aetopoulou I. Photocatalytic degradation of the textile dye reactive orange 16 in the presence of TiO_2 suspensions. Environ Technol 1999;20:479-87.
6. Luo S, Wang R, Yin J, Jiao T, Chen K, Zou G, *et al*. Preparation and dye degradation performances of

self-assembled MXene-Co_3O_4 nanocomposites synthesized via solvothermal approach. ACS Omega 2019;4:3946-53.
7. Salama A, Mohamed A, Aboamera NM, Osman TA, Khattab A. Photocatalytic degradation of organic dyes using composite nanofibers under UV irradiation. Appl Nanosci 2018;8:155-61.
8. Sacco O, Stoller M, Vaiano V, Ciambelli P, Chianese A, Sannino D. Photocatalytic degradation of organic dyes under visible light on N-doped TiO_2 photocatalysts. Int J Photoenergy 2012;2012:1-8.
9. Stylidi M, Kondarides DI, Verykios XE. Pathways of solar light-induced photocatalytic degradation of azo dyes in aqueous TiO_2 suspensions. Appl Catal B Environ 2003;40:271-86.
10. Wu Z, Chen X, Liu X, Yang X, Yang Y. A ternary magnetic recyclable ZnO/Fe_3O4/g-C_3N_4 composite photocatalyst for efficient photodegradation of monoazo dye. Nanoscale Res Lett 2019;14:147.
11. Barathi D, Rajalakshmi N, Ranjith R, Sangeetha R, Meyvel S. Controllable synthesis of CeO_2/g-C_3N_4 hybrid catalysts and its structural, optical and visible light photocatalytic activity. Diam Relat Mater 2021;111:108161.
12. Yang Y, Sun M, Zhou J, Ma J, Komarneni S. Degradation of orange II by Fe@Fe_2O_3 core shell nanomaterials assisted by $NaHSO_3$. Chemosphere 2020;244:125588.
13. Ho C, Yu JC, Kwong T, Mak AC, Lai S. Morphology-controllable synthesis of mesoporous CeO_2Nano- and microstructures. Chem Mater 2005;17:4514-22.
14. Tuprakay S, Liengcharernsit W. Lifetime and regeneration of immobilized titania for photocatalytic removal of aqueous hexavalent chromium. J Hazard Mater 2005;124:53-8.
15. Antón-García D, Edwardes Moore E, Bajada MA, Eisenschmidt A, Oliveira, AR. Photoelectrochemical hybrid cell for unbiased CO_2 reduction coupled to alcohol oxidation. Nat Synth 2022;1:77-86.
16. Channei D, Inceesungvorn B, Wetchakun N, Phanichphant S, Nakaruk A, Koshy P, *et al*. Photocatalytic activity under visible light of Fe-doped CeO_2 nanoparticles synthesized by flame spray pyrolysis. Ceram Int 2013;39:3129-34.
17. Xuan S, Jiang W, Gong X, Hu Y, Chen Z. Magnetically separable Fe_3O_4/TiO_2 hollow spheres: Fabrication and photocatalytic activity. J Phys Chem C 2009;113:553-8.
18. Beydoun D, Amal R, Low GK, McEvoy S. Novel photocatalyst: Titania-coated magnetite. Activity and photodissolution. J Phys Chem B 2000;104:4387-96.
19. Mei Y, Zeng J, Sun M, Ma J, Komarneni S. Funders A novel fenton-like system of Fe_2O_3 and $NaHSO_3$ for Orange II degradation. Sep Purif Technol 2020;230:115866.
20. Nguyen LT, Nguyen HT, Nguyen LT, Duong AT, Nguyen HQ, Ngo VT, *et al*. Efficient and recyclable Nd^{3+}-doped $CoFe_2O_4$ for boosted visible light-driven photocatalytic degradation of Rhodamine B dye. RSC Adv 2023;13:10650-6.
21. Venugopal G, Krishnamoorthy K, Mohan R, Kim SJ. An investigation of the electrical transport properties of graphene-oxide thin films. Mater Chem Phys 2012;132:29-33.
22. Suk JW, Piner RD, An J, Ruoff RS. Mechanical properties of monolayer graphene oxide. ACS Nano 2010;4:6557-64.
23. Saravanan R, Karthikeyan S, Gupta VK, Sekaran G, Narayanan V, Stephen A. Enhanced photocatalytic activity of ZnO/CuO nanocomposite for the degradation of textile dye on visible light illumination. Mater Sci Eng C Mater Biol Appl 2013;33:91-8.
24. Lu T, Zhang R, Hu C, Chen F, Duo S, Hu Q. TiO_2-graphene composites with exposed {001} facets produced by a one-pot solvothermal approach for high performance photocatalyst. Phys Chem Chem Phys 2013;15:12963-70.
25. Satyam Naidu K, Annapurna N. Synthesis, characterization and magnetic properties of iron oxide nanoparticles from reverse chemical co-precipitation method. J Phys Conf Ser 2024;2765:012024.
26. Gomathi A, Prabhuraj T, Gokilapriya S, Vasanthi G, Maadeswaran P, Ramesh Kumar KA. Design of ternary CeO_2/Fe2O_3/reduced graphene oxide-based hybrid nanocomposite for superior photocatalytic degradation material for organic dyes. Dyes Pigm 2023;218:111473.

Source of Support: Nil. **Conflicts of Interest:** None declared.